Earth and Space Science

RESEARCH ARTICLE
10.1029/2019EA000984

Environmental Lapse Rate for High-Resolution Land Surface Downscaling: An Application to ERA5

Emanuel Dutra[1], Joaquín Muñoz-Sabater[2], Souhail Boussetta[2], Takuya Komori[3], Shoji Hirahara[3], and Gianpaolo Balsamo[2]

[1]Instituto Dom Luiz (IDL), Faculdade de Ciências, Universidade de Lisboa, Lisbon, Portugal, [2]European Centre for Medium-Range Weather Forecasts, Reading, UK, [3]Global Environment and Marine Department, Japan Meteorological Agency, Tokyo, Japan

Key Points:
- Environmental lapse rate derived from atmospheric reanalysis vertical profiles agrees with observational estimates
- Surface downscaling outperforms ERA5, but the impact of different ELR corrections to the driving data is reduced
- Systematic biases in ERA5 near-surface temperature require further efforts from modeling and data assimilation

Supporting Information:
- Supporting Information S1

Correspondence to:
E. Dutra,
endutra@fc.ul.pt

Citation:
Dutra, E., Muñoz Sabater, J., Boussetta, S., Komori, T., Hirahara, S., & Balsamo, G. (2020). Environmental lapse rate for high-resolution land surface downscaling: An application to ERA5. *Earth and Space Science*. 7, e2019EA000984. https://doi.org/10.1029/2019EA000984

Received 4 NOV 2019
Accepted 16 FEB 2020
Accepted article online 19 APR 2020

Abstract In this study we derive the environmental lapse rate (ELR) from vertical profiles of temperature in the lower troposphere, applying it to downscale air temperature of the new European Centre For Medium-Range Weather Forecasts (ECMWF) reanalysis ERA5, which replaces ERA-Interim (ERAI). We focus over the western U.S. region, a data-rich area with observations of daily maximum and minimum temperature (Global Historical Climatology Network) and snow depth and soil temperature. Observations indicate an ELR of -4.5 K·km^{-1} in the region, lower than the commonly used -6.5 K·km^{-1}. ERA5 ELR agrees with the observational estimates, with some overestimation in winter and limitations in the diurnal variability. The elevation correction of ERA5 temperature using different ELR showed the benefits of deriving ELR fields from ERA5 vertical profiles, when compared with a constant ELR. Simulations with the ECMWF land surface model, at 9-km resolution, driven by ERA5 using different ELR corrections showed the added value of the methodology, but the impact of different ELR corrections is limited. However, the validity of the downscaling method in reducing temperature to station altitude suggests that there is sufficient generality for application at kilometer and subkilometer resolutions. By comparing the estimated representativity errors of observations with reanalysis, the improvements from ERAI to ERA5 are mainly visible in the random component of the error. Large systematic biases remain, which require further attention from the modeling and data assimilation, and limit the potential benefits of ELR corrections.

1. Introduction

High spatial and temporal resolution near-surface climate and weather conditions are paramount for the understanding, monitoring, and forecasting of ecological, hydrological, and climate change processes, among others (e.g., Behnke et al., 2016; Maraun et al., 2010; Maselli et al., 2012; Tobin et al., 2012). Near-surface air temperature and precipitation are key fields due to their relevance in the evolution of surface and subsurface conditions (e.g., vegetation and groundwater), which are then used to drive process-based or statistical models. High spatial resolution is also becoming increasingly important in climate change studies with examples such as the Coordinated Regional Climate Downscaling Experiment (e.g., Endris et al., 2013; Soares et al., 2017). A common approach to enhance the spatial resolution is statistical or dynamical downscaling. Statistical downscaling can be very effective, in particular if using local observations (e.g., Cao et al., 2017; Maraun et al., 2010; Winstral et al., 2017). Dynamical downscaling of global atmospheric reanalysis, weather forecasts, or climate change projections is a widely used methodology to enhance the spatial information (Soares et al., 2012). Dynamical downscaling with limited area (or regional) atmospheric models has a significant computational cost but provides a physically consistent description of the land and atmosphere (e.g., relation between temperature, humidity, radiation, clouds, and precipitation), while suffering from model limitations (e.g., biases). Statistical downscaling is based on statistical relationships to predict the evolution of local variables from large-scale variables. It is computationally cheaper but requires observations, which are not always available, and the spatial consistency between downscaled fields can be difficult to achieve.

Temperature near the surface varies with altitude accordingly to the environmental lapse rate (ELR). The ELR depends on the overlying air masses, large-scale situation, and local effects (Sheridan et al., 2010). The characterization of the ELR has several applications, in particular to downscale global/regional numerical

weather predictions, reanalysis, and climate projections in complex terrain regions. From an observational point of view, complex terrain regions also constitute a challenging environment due to the difficulties associated with the installation and maintenance of observational networks. The use of a linear lapse rate for altitude correction of temperature is a common practice (e.g., Dodson & Marks, 1997). The main challenge is the definition of the ELR. Optimally, provided that there is a high density and homogeneous distribution of stations, this information could be used. However, such station density is not available globally. Accounting for elevation differences is fundamental for temperature interpolations over complex terrain regions (Stahl et al., 2006). There are numerous observational indications that ELR varies in time and space and that the commonly used constant value of $-6.5\ K{\cdot}km^{-1}$ is to high (e.g., Jobst et al., 2017; Minder et al., 2010; Shen et al., 2016; Wang et al., 2018). Without local observations spanning a wide range of altitude bands, atmospheric vertical profiles have also been used to estimate the ELR. Gao et al. (2012) evaluated several ELR in the Alps using station information. They found that compared with a constant climatology (Liston & Elder, 2006), the ELR derived from the pressure levels of ERA-Interim (ERAI) atmospheric reanalysis (Dee er al., 2011) had a good performance. This methodology was also found to perform well when tested in the Tibetan Plateau (Gao et al., 2017; Gerlitz et al., 2014).

The use of ELR for elevation corrections between model and station temperature is widely accepted, but other surface characteristics such as snow depth or soil temperature are also expected to depend significantly with altitude. Model simulations with a land surface model (hereafter surface simulations) forced with downscaled near-surface meteorology can be a compromise to enhance the spatial resolution but with a considerable lower computational cost when compared with a dynamical downscaling using a regional or limited area atmospheric model. Bernier et al. (2011) carried out surface simulations at 100-m resolution in a complex Alpine region in Vancouver Canada showing the added value of this methodology in simulating snow evolution. This was further investigated by Ioannidou et al. (2014) to evaluate surface winds downscaling.

In this study we aim to evaluate the effect and impact of different ELR corrections to downscale the new European Center for Medium-Range Weather Forecasts atmospheric reanalysis ERA5 (Hersbach et al., 2018). We focus over the western U.S. (WUS) region due to the amount of available observations in the Global Historical Climatology Network-Daily (GHCN), Version 3 (Menne et al., 2012), and the Natural Resources Conservation Service (NRCS) SNOTEL network, as well as its complex terrain characteristics. As a first step, estimates of the ELR were derived from observations of daily maximum, minimum, and mean temperature, and then, ERA5 temperature was reduced to the station's altitude using different ELR corrections. The ELR corrections include a constant ELR commonly used of $-6.5\ K{\cdot}km^{-1}$ and spatially and temporally varying ELR fields derived from ERA5 lower troposphere thermodynamic vertical profiles. Surface simulations (or offline) with the European Centre For Medium-Range Weather Forecasts (ECMWF) land surface model HTESSEL were carried out at 9 km driven by ERA5 hourly surface downward fluxes (rainfall, snowfall, longwave, and shortwave radiation) and near-surface state (temperature, specific humidity, wind speed, and pressure). ERA5 fluxes and near-surface state were interpolated to the 9-km resolution, whereas temperature (also humidity and pressure) was corrected for elevation differences between ERA5 (31 km) topography and the 9-km resolution using different ELR corrections. The simulations of snow depth and soil temperature were evaluated and compared with both ERA5 and ERAI. The 9-km resolution was chosen for practical reasons as the highest global resolution currently operationally run at ECMWF; however, this does not represent a limitation of the applicability of the downscaling method. Finally, an estimate of observational uncertainty was performed to assess the role of spatial sampling and altitude variability and compared with ERA5 and ERAI reanalysis. The following section presents the detailed data sets and methodologies, followed by the results with the key conclusions in the last section.

2. Methods

2.1. Data

2.1.1. Observations

The observations of daily maximum temperature (dtmax) and daily minimum temperature (dtmin) were taken from GHCN. GHCN includes daily land surface observations from around the world and from different networks. If observed, the station data set includes dtmax, dtmin, total precipitation, snowfall, and snow depth (Menne et al., 2012). The GHCN data were processed from the original format for the period

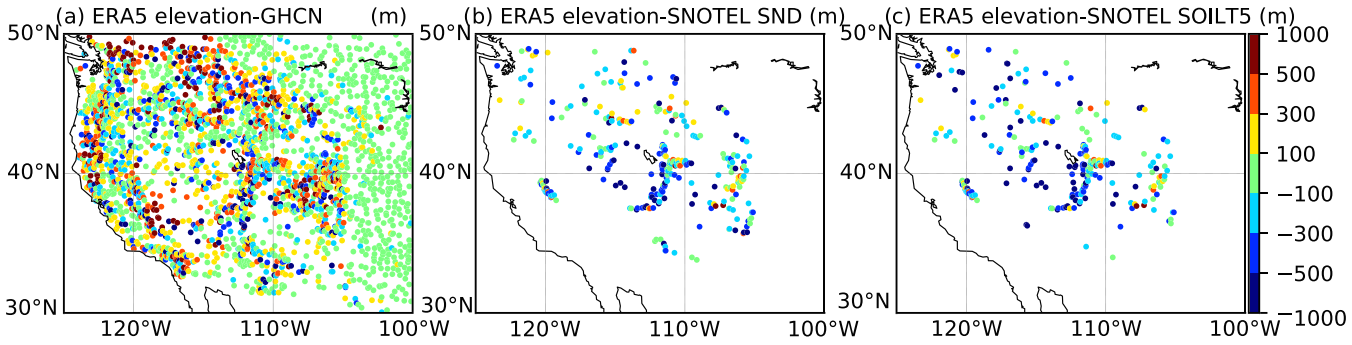

Figure 1. ERA5 orography differences in respect to the stations elevation of GHCN (a), SNOTEL snow depth (b), and SNOTEL soil temperature (c).

1 June 2009 to 31 May 2014 restricting the data to a region between 125° to 100° west and 30° to 50° north (WUS). This region was selected due to the high density of stations and elevation variability. A missing data screening was applied to retain only stations with at least 80% of available data for the period considered. After the regional and temporal filters, 2,941 stations were retained (Figure 1a) with dtmin and dtmax data with at least 80% of available data for the 5 years considered. The daily mean temperature (dtmean) was also considered in the analysis. Since dtmean is not available in GHCN, it was computed as the arithmetic mean between Tmin and Tmax. This simple approach can lead to some deviations from the actual daily mean temperature (Dall'Amico & Hornsteiner, 2006; Weiss & Hays, 2005). However, since GHCN only contains dtmin and dtmax, the simplest option for the daily mean computation was selected.

In addition to the GHCN air temperature observations, the NRCS SNOTEL network observations of snow depth and soil temperature at 5-cm depth were used in the model evaluation. The observations were processed for the same time period and region as GHCN, retaining only stations with 80% of available daily data. This resulted in 313 stations with snow depth (Figure 1b) and 260 stations with soil temperature (Figure 1c). The soil temperature data from this network has been used to evaluate ECMWF soil temperature performance (Albergel et al., 2015). The GHCN data set also includes snow depth, but only the NRCS-SNOTEL network was used in this study. This network has been designed to collect snow and climate data in WUS mountainous regions, which is the environment expected to be mostly affected by model topography and resolution.

2.1.2. Reanalysis

In this study we focus on the the most recent ECMWF atmospheric reanalysis ERA5 (Hersbach et al., 2018). This is the latest and fifth generation of atmospheric reanalysis produced by ECMWF under the Copernicus Climate Change Service. This new reanalysis replaces the widely used ERA-Interim reanalysis (Dee et al., 2011) from 1979 to close to real time as well as an extension back to 1950. Compared with ERAI, ERA5 has several enhancements, including (i) higher spatial horizontal resolution (about 75 km in ERAI to 31 km in ERA5), (ii) higher vertical resolution (from 60 levels in ERAI to 137 in ERA5), (iii) higher temporal resolution of archived data (3-hourly in ERAI to hourly in ERA5), and (iv) a recent model and data assimilation systems. Regarding the model and assimilation changes, there are numerous improvements benefiting from more than 10 years of development of the numerical weather prediction system at ECMWF. For example, the land surface scheme has suffered a major upgrade that leads to a land-only interim reanalysis ERA-Interim/Land (Balsamo et al., 2015), including a revised soil hydrology (Balsamo et al., 2009) and snow scheme (Dutra et al., 2010). Other examples of model changes include revisions in the convection and diffusion (Bechtold et al., 2008). ERA5 dtmin and dtmax were calculated from the 2-m temperature hourly analysis, and dtmean was computed as the arithmetic mean of dtmin and dtmax to be consistent with the processing of GHCN.

2.2. ELR Estimates

The ELR is defined as the rate of temperature change with height and can be computed as follows:

$$\Gamma = \frac{DT}{DZ}, \tag{1}$$

where Γ is the ELR ($K \cdot km^{-1}$) and DT is the temperature difference (K) between two layers DZ, assuming 0 at the land surface. Γ is normally negative with a lower limit of -10 $K \cdot km^{-1}$ for the dry-adiabatic lapse rate,

taking higher values with increased moisture. In particular situations, the ELR can take positive values; that is, temperature increases with height leading to temperature inversions. These situations occur mainly in stable conditions or due to large-scale subsidence.

2.2.1. Observations

The ELR was estimated from the in situ GHCN observations via linear regression of the observed temperature versus the station altitude in the form

$$T_i = \Gamma_O \times Z_i + T_0, \tag{2}$$

where T_i (K) is the station-observed mean temperature (taken over a specific period) with the associated altitude Z_i (K·m) and the estimated Γ_O is computed by the regression as well as T_0 (the estimated temperature at altitude 0). The temperature averaging period considered included the full 5 years and the mean monthly climatology. Day by day and month by month, calculations were performed, but the regression quality was poor in many areas, which can be associated with synoptic variability affecting each station differently. The linear regression requires the definition of a group of stations. The methodology chosen was to split the study area in a regular grid of 1° by 1° and to perform the regression for all stations falling within each area with a 2° search radius. This leads to some overlap; that is, one station can be used in several area calculations. Only points with at least 30 stations and with a standard deviation of the stations altitude higher than 400 m were considered. These two constraints were imposed to guarantee a robust linear regression. Furthermore, only regressions with a coefficient of determination (R^2) above 0.5 were considered to mask out problematic areas (e.g., snow vs. snow free, highly inhomogeneous areas, and coastal areas). This approach transforms the spatial distribution of surface temperature for different stations in each 1° by 1° area into an estimate of ELR. This approach has two main limitations: (i) it relies on the elevation variability among the stations, and (ii) it assumes that temperature at stations in different elevations is representative of the mean lower troposphere vertical structure. Sounding data could be used also to derive the ELR, but since most of the freely available sounding data have been used by the data assimilation in ERA5, this would likely result in similar estimates as those derived from ERA5 vertical profiles.

2.2.2. Reanalysis

The ELR was estimated from the temperature vertical profiles of ERA5 in the lower troposphere. A similar methodology to derive the ELR was proposed by Gao et al. (2012, 2017) over the French Alps and Tibetan Plateau for temperature elevation corrections. Gao et al. (2017) estimated the ELR from the temperature differences between different pressure levels. We propose a modification using the original model levels that follow the model topography. We compute the ELR as in equation (1) between 16 combinations of model levels centered between model level 124 (500 m above the surface) and model level 116 (1,200 m above the surface). These 16 estimates of the ELR are then averaged, considering only negative values, that is, excluding temperature inversions. Several combinations of upper and lower limits were tested, and the levels between 500 to 1,200 m were chosen to avoid sharp inversions near the surface as well as subsidence inversions. Even with the limits at 500 and 1,200 m, inversions are captured, and an ELR of 0 is assumed in those situations. On a global scale, the main regions with positive (set to 0) ELR are associated with large-scale subsidence linked with either the Hadley circulation (over the oceans) or winter anticyclonic subsidence and very stable conditions in northern latitude land masses.

The ELR was estimated using the vertical profiles of temperature and specific humidity (the latter required to compute the altitude from the model levels), using two time periods averaging (i) daily means of the analysis at 0/6/12/18 UTC resulting in daily global fields of ELR (daily ELR) and (ii) the 5-year mean monthly analysis resulting in one global field for each calendar month (mean climatological ELR). In addition to these two methods (see Table 1), a globally and temporally constant ELR of -6.5 K·km^{-1} (clr) and -4.5 K·km^{-1} (clrO) was also included. The constant value of -6.5 K·km^{-1} is widely used in many applications (e.g., Cosgrove et al., 2003; Maurer et al., 2002) derived from estimates of the mean free-atmosphere lapse rate. The constant ELR of -4.5 K·km^{-1} was taken from the observation estimates (see section 3.1).

2.3. Land Surface Simulations

The ERA5 lowest model level (about 10-m height) fields of air temperature, specific humidity, wind speed, and surface pressure along with the downwelling fluxes of shortwave and longwave radiation and solid and liquid precipitation were used to perform surface (or offline) simulations. We use the same land surface model version as used in ERA5, which is very similar to the version used for ERA-Interim/land

Table 1
Acronyms and Description of the Elevation Correction of ERA5 Temperature (Top Rows) and HTESSEL Land Surface Simulations (Bottom Rows)

Acronym	Description
clr	Elevation correction of ERA5 temperature using a constant ELR of -6.5 K·km^{-1}
clr0	Elevation correction of ERA5 temperature using a constant ELR of -4.5 K·km^{-1}
mlr	Elevation correction of ERA5 temperature using mean monthly climatological ELR fields derived from ERA5 vertical profiles
dlr	Elevation correction of ERA5 temperature using daily ELR fields derived from ERA5 vertical profiles
HTbil	HTESSEL land surface simulation at 9 km driven by ERA5 hourly downward fluxes (rainfall, snowfall, longwave, and shortwave radiation) and near-surface state (temperature, humidity, wind, and pressure). Bilinear interpolation of ERA5 fields from 31 to 9 km.
HTclr	As HTbil but adjusting ERA5 temperature, humidity, and pressure using a constant ELR of -6.5 K·km^{-1}
HTmlr	As HTclr but using a mean monthly climatology of ELR fields
HTdlr	As HTclr but using daily ELR fields
HTei	As HTbil but using 3-hourly ERA-Interim downward fluxes and near-surface state. Bilinear interpolation of ERA-Interim fields from 75 to 9 km.

(Balsamo et al., 2015). The ERA5 meteorological fields are taken from the +1h to +12h forecasts initialized at 06 UTC and 18 UTC, resulting in continuous hourly time series.

The surface simulations were performed at a higher resolution than ERA5, matching that of ECMWF high-resolution weather forecasts of about 9 km. The simulations were initialized in January 2009 extending until May 2014. The first 5 months of simulation were considered as spin-up. Since the evaluation focuses only on near-surface variables, possible effects of spin-up (e.g., adjustment of deep soil moisture/temperature) have a small impact. Four simulations were performed differing on the meteorological forcing and are listed in Table 1. The default configuration is bilinear interpolation of the forcing fields (HTbil) while the remaining three were adjusted to the differences between ERA5 (31 km) and the high-resolution (9 km) model orography using different ELR estimates. The corrections are the following: (i) Relative humidity is computed from the uncorrected forcing; (ii) air temperature is corrected using the ELR and altitude difference; (iii) surface pressure is corrected assuming the altitude difference and updated temperature; and (iv) specific humidity is computed using the new surface pressure and temperature assuming no changes in relative humidity.

One additional simulation was carried out for the same period using ERAI forcing and resolution (about 75 km) (hereafter HTei). HTei has the same configuration as ERA-Interim/Land but used the same model version as ERA5, and there was no precipitation correction as in ERA-Interim/Land. Despite the similarities, this new simulation was performed to guarantee that all surface simulations presented in this study were carried out with the same model version and consistent with ERA5.

2.4. Evaluation Metrics

In the simulations evaluation four main scores are used: (i) the mean bias (simulation-observation [BIAS]); (ii) the mean absolute error (MAE); (iii) the standard deviation of the error (standard deviation of the differences between the simulation and observation [STDE]); and (iv) the temporal correlation (PCORR). While the BIAS and MAE indicate systematic errors, the STDE (also known as the unbiased root-mean-square error) can be interpreted as the random component of the error. The scores are computed for each station and considered time period. The metrics are presented as the median of the scores of all stations to avoid outliers, which could affect the mean of the score. Confidence intervals of the median scores were estimated with a 1,000-sample bootstrapping with replacement to account for stations sampling uncertainty.

2.5. Observations Representativity

The representativity of the in situ temperature observations was estimated by computing the MAE and STDE of each station against the mean over a certain radius. The calculation was performed in the following steps:

1. For each individual station, a group of stations was created with a distance smaller than a particular radius (area).
2. The spatial mean of all stations in that radius was computed to represent area mean. This included two calculations: (i) including all stations and (ii) including only stations with a similar altitude, defined as altitude within ±100 m from the mean in the area.
3. The MAE and STDE were computed for each station against the area mean computed in (2). Steps 1–3 were repeated for all stations and search radius from 30 to 150 km.

Only areas (in Point 1) with at least 10 stations were retained, and the number of areas and mean number of stations in each region was saved. Since the areas are defined starting from each station, there is a significant overlap; that is, the same stations are accounted in several regions. This procedure can be seen as a smoothing filter to generate the area means that are then used to compute the MAE and STDE as measures of the spatial representativity of the observations. The restrictive selection criteria of similar altitude stations were introduced to estimate how much of the representativity errors can be associated with altitude differences.

3. Results

3.1. ELR From Observations and Reanalysis

The high-density temperature observation and terrain variability in the WUS region allow the estimation of the ELR based on in situ stations. Figure S1 in the supporting information shows the station spatial distribution as well as the aggregated number of stations, mean elevation, and standard deviation of the station elevation in each of the regular areas considered. The restriction of at least 30 stations with elevation variability, measured by the standard deviation, excluded mostly the eastern region of WUS domain due to the reduced elevation variability.

The observational estimates of the ELR show a clear annual cycle (Figure 2d). Daily ELR estimates were calculated, but the results were noisy, which could be related to the different times of occurrence of the temperature extremes in each station. The temporal averages considered in the study (e.g., all days in each calendar month; Figure 2d) filter out the random timing differences resulting in consistent temporal (mean climatology) and spatial fields, comparable with the independent estimates from ERA5. The estimates depend on the variable taken: lower absolute ELR when using the daily minimum temperature and higher absolute ELR when using the daily maximum temperature. These results are expected since nocturnal low-level conditions tend to be more stable, resulting in less intense ELR when using the daily minimum temperature. The comparison between observations and ERA5 ELR shows a reasonable agreement when considering the spatial averages over the domain (Figure 2d). The south-north gradient is also captured (annual fields in Figures 2e and 2f and Figure S2 for the winter and summer months). The mean absolute difference of the ERA5 ELR compared with the station estimates is 1.5 (2), 1.2 (3.1), and 1.8 (1.5) $K \cdot km^{-1}$ for the annual, winter, and summer periods, respectively (between brackets are the mean absolute differences of a constant ELR of −6.5 compared with the station estimates). The linear regression slopes in Figures 2a to 2c are always below 1 suggesting a reduced sensitivity of ERA5 ELR compared with the observational estimates. During summer, ERA5 ELR estimates have a small sensitivity for large absolute ELR with a general overestimation (Figure 2b), which is also present in the annual ELR (Figure 2a), but less pronounced. This is particularly evident in the northern area of the domain. Further analyses did not identified any particular characteristic that could explain these differences. It is likely that some of the differences arise from the uncertainties introduced by different assumptions used to derive the ELR from ERA5 vertical profiles and from the spatial and vertical variability of the station observations.

3.2. Elevation Correction of ERA5 Temperature

Meteorological stations are usually located in easily accessible areas, resulting in a sampling bias of lower altitudes when considering the local topography. This is illustrated when comparing the altitude differences, defined as the differences between ERA5 orography and the station elevation (see Figures 1a and S3b), with a higher frequency of stations below ERA5 orography than above. In this section we compare ERA5 dtmin, dtmean, and dtmax with ERA5 temperatures reduced to the station elevation using different ELR

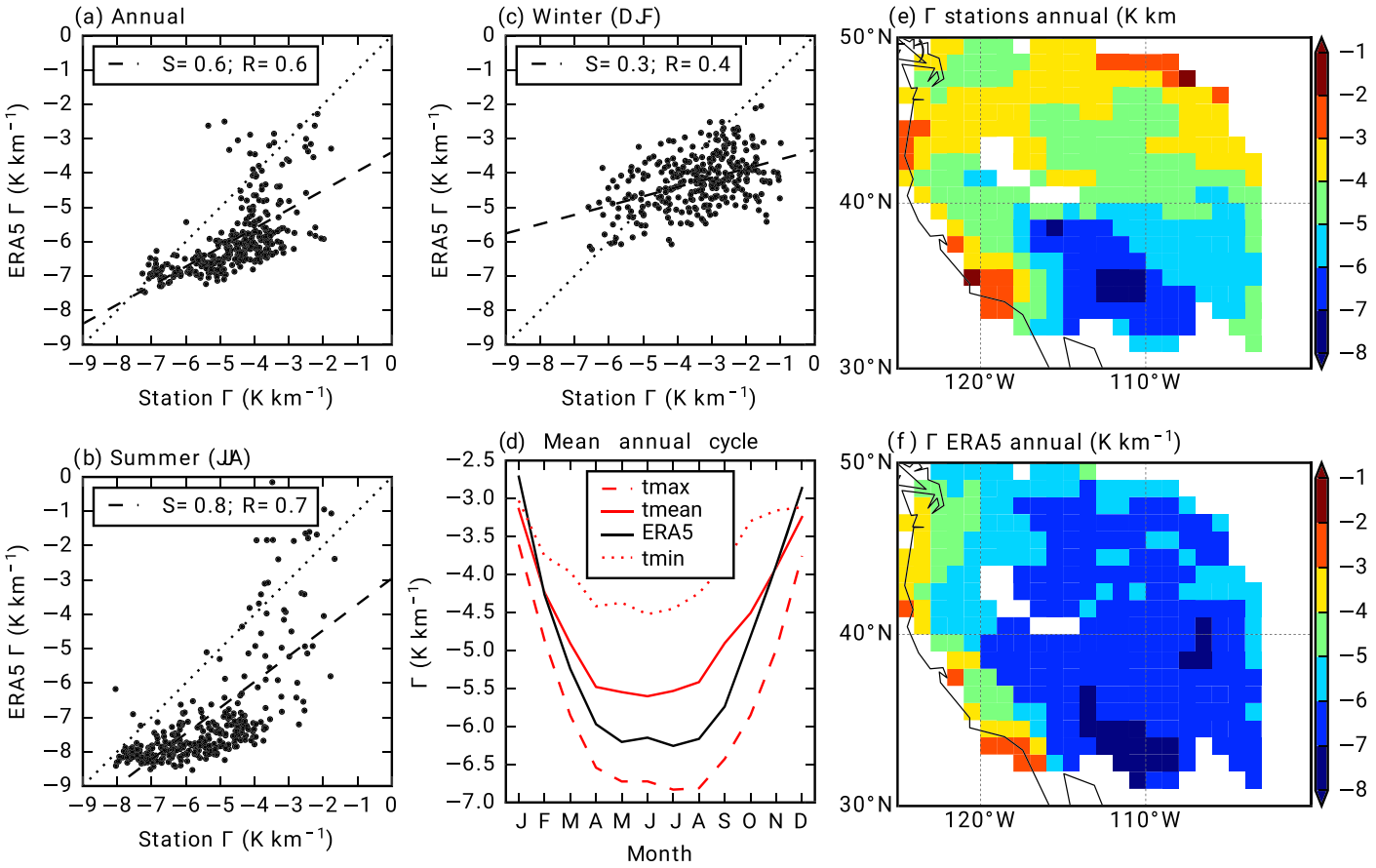

Figure 2. Comparison of ELR (Γ) derived from ERA5 vertical profiles and estimated from the station observation over the WUS domain. ERA5 versus dtmean station ELR for each grid point considering the full period (a) (June 2009 to May 2014), summer (b), and winter (c). (d) Mean annual cycle of ELR averaged over WUS domain given by ERA5 (black line) and station data computed with dtmax (dashed red), dtmean (solid red), and dtmin (dotted red). Spatial distribution of ELR for the full period using dtmean from the station data (e) and ERA5 (f). In panels (a)–(c) the slope of the linear fit (*S* and dashed line) and correlation coefficient (*R*) are displayed in the legend.

corrections: constant lapse rate of −6.5 and −4.5 K·km^{-1} (clr and clrO), monthly climatology fields of ELR derived from ERA5 (mlr), and daily ELR fields derived from ERA5 (dlr). The temperature differences, defined as the difference between model and observations, when organized as function of the elevation differences highlight the role of elevation in the mean bias (Figure 3). The slope of the linear regression between these temperature differences as function of elevation differences can be also interpreted as an estimate of the ELR required to correct model data, and the correlation coefficient a measure of the linear dependence. The dependence of ERA5 mean temperature bias on elevation differences is clear for dtmax and dtmean while for dtmin, the relation is not so strong (Figure 3 and Table 2; note the higher correlations for dtmax and dtmean when compared with dtmin). This is further illustrated when considering only summer or winter months (Table 2). These results indicate that the bias relation with altitude is not constant (or the ELR required to correct model data). Taking dtmean for the full period, the optimal ELR correction for the region is −4.5 K·km^{-1}. Considering the different ELR corrections, none consistently outperforms the others. The dlr and mlr provide the best corrections for dtmean consistently for the full period or when considering only winter or summer months. In general, all corrections fail to capture the high ELR for dtmax and low ELR for dtmin.

The added value of the ELR correction to ERA5 is clear for dtmax (see Figure 4) in terms of a reduction of the mean absolute error and bias. For the standard deviation of the error, there is no change in case of a constant ELR, but the time-varying ELR (dlr or mlr) increases the error. There is no clear added value of a variable ELR correction when compared with an optimal constant ELR (clrO—derived for this area as −4.5 K·km^{-1}) when considering all stations and these metrics. Independently from the ELR chosen, the corrections for

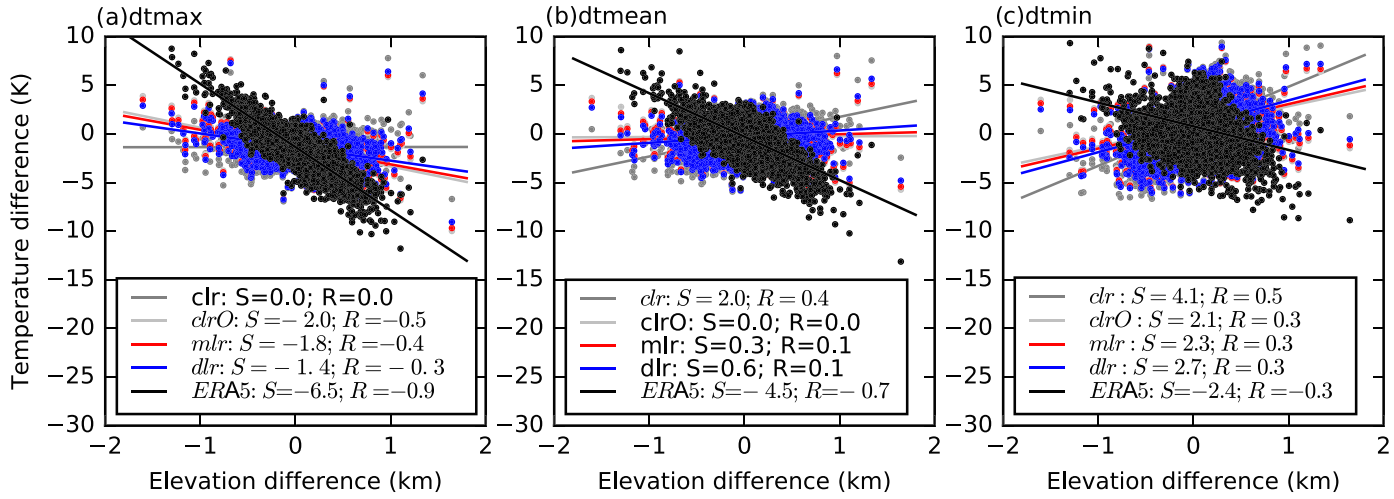

Figure 3. Temperature differences between ERA5 and observations as a function of the station elevation differences (ERA5 station) for dtmax (a), dtmean (b), and dtmin (c) considering the full period. The scatter plots display ERA5 (black), ERA5 with a constant Γ correction of −6.5 K·km^{-1} (clr, gray), ERA5 with a constant Γ correction of −4.5 K·km^{-1} (clrO, light gray), ERA5 with a climatological Γ correction (mlr, red), and ERA5 with a daily Γ correction (blue). In each panel the legend displays the slope (S) of the linear best fit and correlation coefficient (R).

dtmax and dtmean are always positive and more pronounced during summer when compared with winter. For dtmin, the ELR corrections are neutral or detrimental, which is consistent with the previous analysis of the temperature bias relationship with elevation differences (Figure 3). If we consider only stations above or below ERA5 orography (see Figure 5 for the bias and Figures S4 and S5 for the remaining scores), the results highlight a large discrepancy in the correction impact. For stations above model orography (Figures 5a–5c), all ELR corrections reduce the temperature biases during summer while deteriorate during winter, with clr being the worst. While, during summer, ERA5 has a warm bias in these stations, which is expected, there was a neutral to negative bias during winter. The ELR correction leads to a cold bias, which is then reflected in the MAE deterioration. Considering only the stations below ERA5 orography (valley stations, Figures 5d–5f), the ELR corrections are effective for dtmax and dtmean with average reductions of 40% of the MAE. For dtmin, the improvements are smaller with even some deterioration during summer. In these valley stations, ERA5 shows a strong cold bias (almost −5 K) for dtmax and a much smaller cold bias for dtmin (about −1.3 K), suggesting an underestimation of the amplitude of the diurnal cycle, which is independent from the relative elevation difference from ERA5 and likely related with local effects.

Table 2
Statistics of the Linear Regression Between Elevation Differences and Temperature Differences for the Different ELR Adjustments and ERA5 Original Data for the Entire Period (ALL) and Winter and Summer

	ALL					Winter (DJF)					Summer (JJA)				
	ERA5	clr0	clr	mlr	dlr	ERA5	clr0	clr	mlr	dlr	ERA5	clr0	clr	mlr	dlr
dtmax	−6.5	−2.0	**0.0**	−1.8	−1.4	−4.2	**0.3**	2.3	−1.3	−0.7	−7.8	−3.3	−1.3	−2.1	−1.8
	−0.9	−0.5	**0.0**	−0.4	−0.3	−0.6	**0.1**	0.4	−0.2	−0.4	−0.9	−0.6	−0.3	−0.5	−0.4
dtmean	−4.5	**0.0**	2.0	**0.3**	**0.6**	−2.8	1.7	3.7	**0.1**	**0.6**	−5.5	−0.8	1.2	**0.4**	**0.7**
	−0.7	**0.0**	0.4	**0.1**	**0.1**	−0.4	0.2	0.5	**0.0**	**0.1**	−0.8	−0.2	0.2	**0.1**	**0.2**
dtmin	−2.4	2.1	4.1	2.3	2.7	−1.4	3.1	5.1	1.5	2.0	−2.8	1.7	3.7	3.0	3.2
	−0.3	0.3	0.5	0.3	0.3	−0.2	0.3	0.5	0.2	0.2	−0.4	0.2	0.4	0.4	0.4

Note. In each cell, the top values denote the slope of the linear regression (K·km^{-1}), and the bottom values denote the correlation coefficient. The bold values highlight corrections with a linear regression slope absolute value below 1 and correlation below −0.4. For each period, the five columns indicate constant ELR of −6.5 K·km^{-1} (clr), constant ELR of −4.5 K·km^{-1} (clrO), mean climatology fields of ELR from ERA5 (mlr), daily ELR fields from ERA5 (dlr), and the original ERA5 data (ERA5).

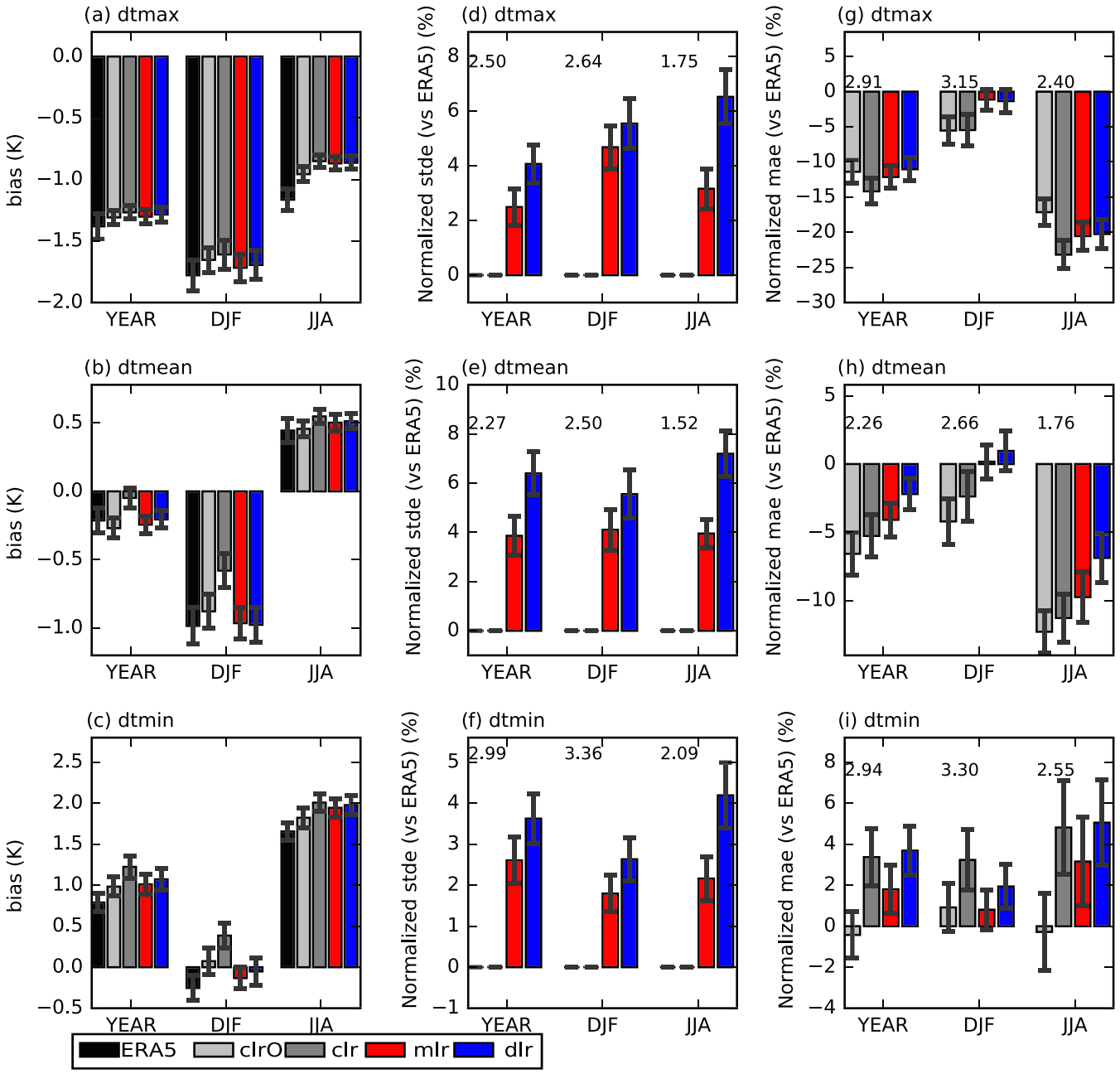

Figure 4. Median bias (a–c), normalized STDE (d–f), and normalized MAE (g–i) of ERA5 and the different ELR corrections of dtmax (top panels), dtmean (middle panels), and dtmin (bottom panels). The bars represent the median of the station scores computed for different periods (horizontal axes: all period—YEAR, DJF, and JJA), and the error bars denote the 95% confidence intervals from 1,000-sample bootstrapping. The STDE and MAE were normalized by those of ERA5, shown above the bars. The statistics were computed using all 2,941 stations with a mean elevation difference between ERA5 orography and stations of 28 m.

3.3. Land Surface Downscaling

The previous sections focused on the near-surface temperature and different approaches to account for station altitude differences in respect to the model orography. Other land surface variables, such as snow depth and soil temperatures, are also expected to vary strongly with altitude as response to air temperature changes. In this section we focus on the SNOTEL snow depth and 5-cm deep soil temperature observations (see Figures 1b and 1c). ERA5 biases in respect to the elevation differences (see Figure S6) show that soil temperature biases are tightly correlated with altitude differences during summer while during winter, this relation is not so evident. In winter, the presence of snow and its thermal insulation effects (Dutra et al., 2011)

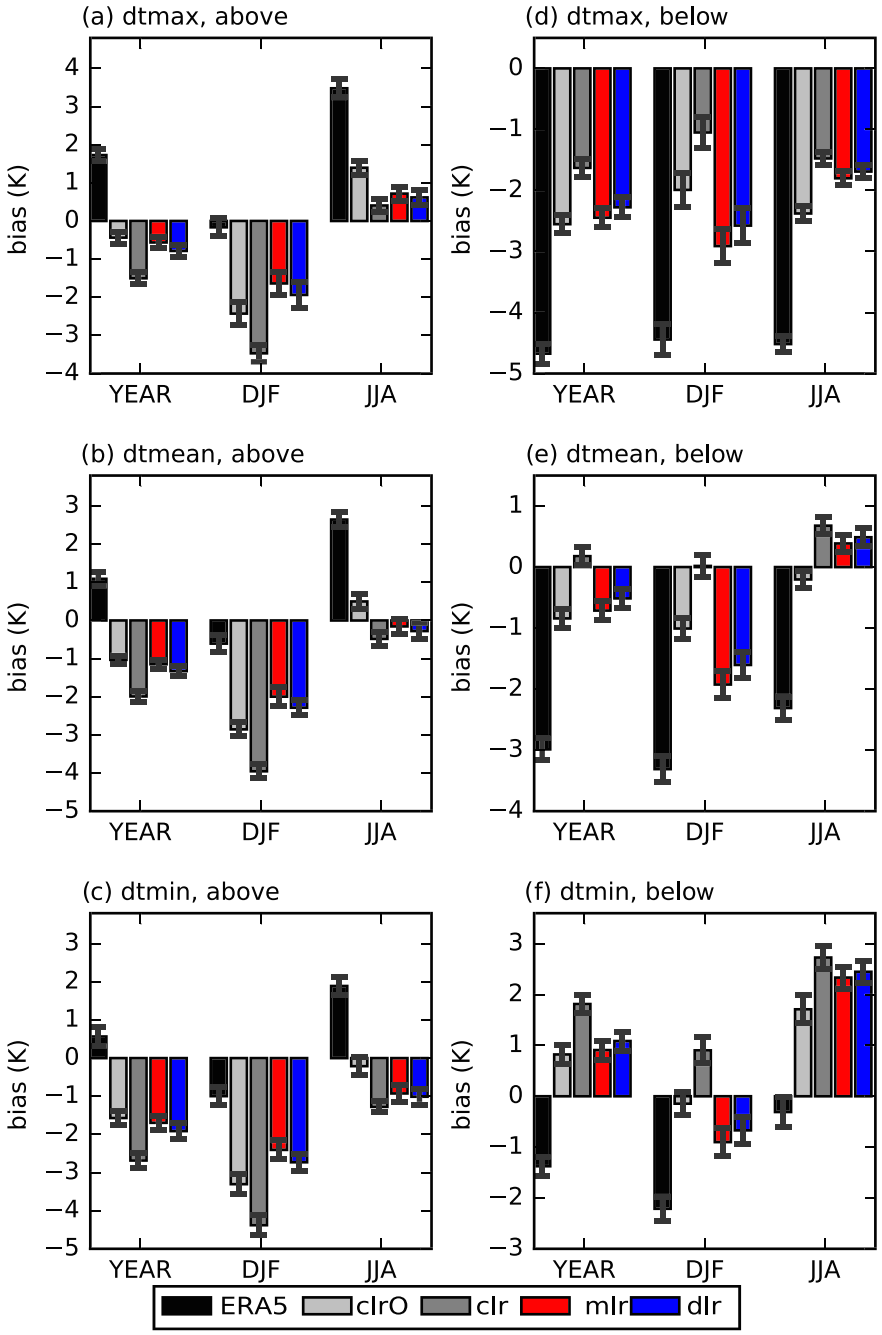

Figure 5. Median bias of ERA5 and the different ELR corrections of dtmax (top panels), dtmean (middle panels), and dtmin (bottom panels), considering stations above ERA5 orography (a–c) (elevation differences >300 m, 385 stations with a mean elevation differences of −475 m) and below ERA5 orography (d–f) (elevation differences <300 m, 494 stations with a mean elevation difference of 450 m). The bars represent the median of the station scores computed for different periods (horizontal axes: all period—YEAR, DJF, and JJA), and the error bars denote the 95% confidence intervals from 1,000-sample bootstrapping. The STDE and MAE were normalized by those of ERA5, shown above the bars.

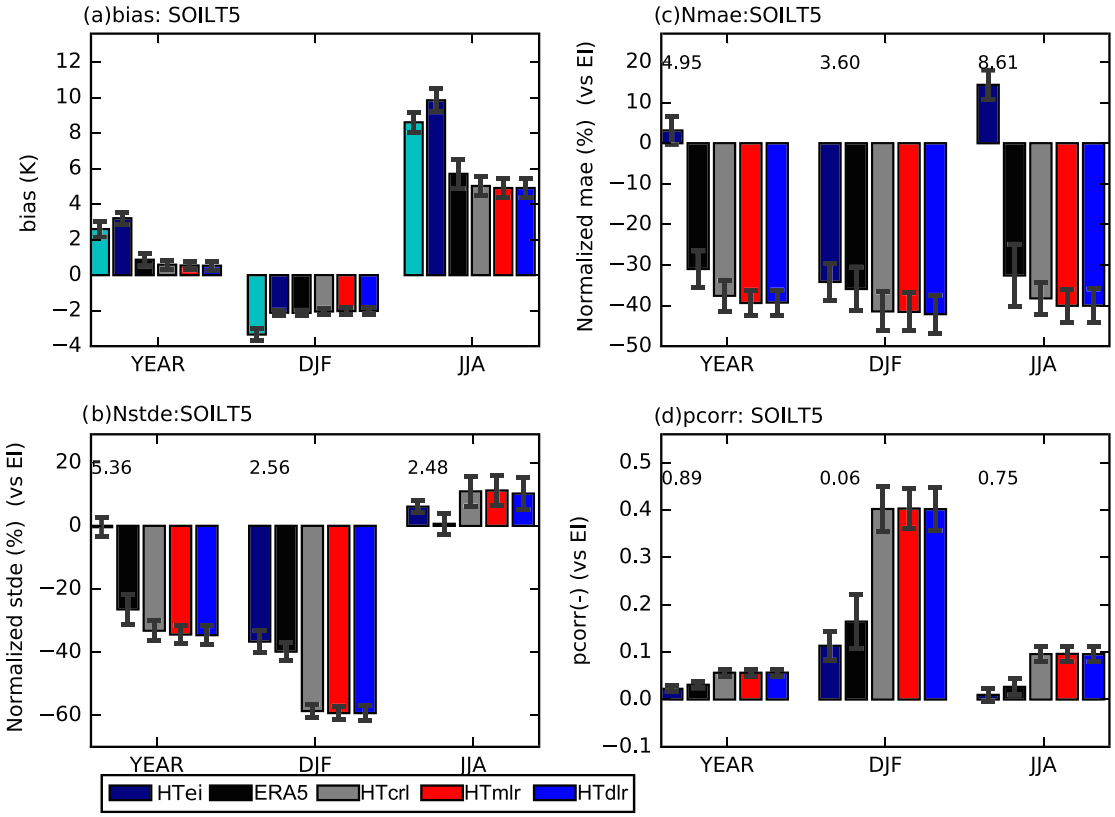

Figure 6. Surface-only simulation evaluation of soil temperature at 5 cm deep: mean bias (a), normalized MAE (b), normalized SDTE (c), and correlation coefficient differences in respect to ERAI (d). The bars represent the median of the station scores computed for different periods (horizontal axes: all period—YEAR, DJF, and JJA), and the error bars denote the 95% confidence interval from 1,000-sample bootstrapping. The MAE and STDE were normalized by those of ERAI, shown above of the bars. In the bias, the light blue bars (first from the left) denote ERAI. The statistics were computed using 260 stations with a mean elevation difference between ERA5 orography and the stations of −460 m.

is likely to dominate over the altitude differences. For snow depth, we see a positive relationship with elevation differences resulting from both temperature effects (colder in altitude) and enhanced precipitation/snowfall with altitude. Considering the tight relationships found between ERA5 biases and observations as functions of altitude differences, in the following results we investigate the potential added value of higher resolution land surface-only simulation with different approaches to account for the ELR in the temperature forcing correction (see Table 1). The results are benchmarked against those of ERAI, including also ERA5 to evaluate the impact of the surface downscaling when compared with the ERAI to ERA5 evolution. Furthermore, an additional surface simulation driven by, and at the same resolution as, ERAI (HTei) but using the same surface model as ERA5 is evaluated to provide the impact of the surface model changes.

The soil temperature evaluation (Figure 6) shows a general improvement from ERAI to ERA5 in all metrics. The added value of the surface downscaling is mainly visible during winter in terms of variability (reduction of 60% of the STDE in respect to ERAI and higher correlations). During winter, HTei also shows some improvements in respect to ERAI (35% reduction of STDE), and similar to ERA5 (45% reduction of the STDE), highlighting the benefits of the model changes from ERAI to ERA5. During summer, the impact on soil temperature of the surface downscaling is smaller than in winter, but there are still some improvements in terms of the MAE and correlation with some deterioration of the STDE. Finally, there is no clear difference between the three tested methods of the ELR temperature correction in terms of soil temperature skill.

The snow depth evaluation (Figure 7) shows a clear evolution from ERAI to HTei with a reduction of the bias, MAE, STDE and increased correlation. ERA5 further improved HTei, which is likely associated with a better meteorology quality (Albergel et al., 2018; Beck et al., 2019). The benefits of the surface downscaling are mainly visible in spring suggesting the added value of the temperature corrections during the ablation season. Taking the spring normalized MAE in respect to ERAI, we see an error reduction of 15% in HTei, 42%

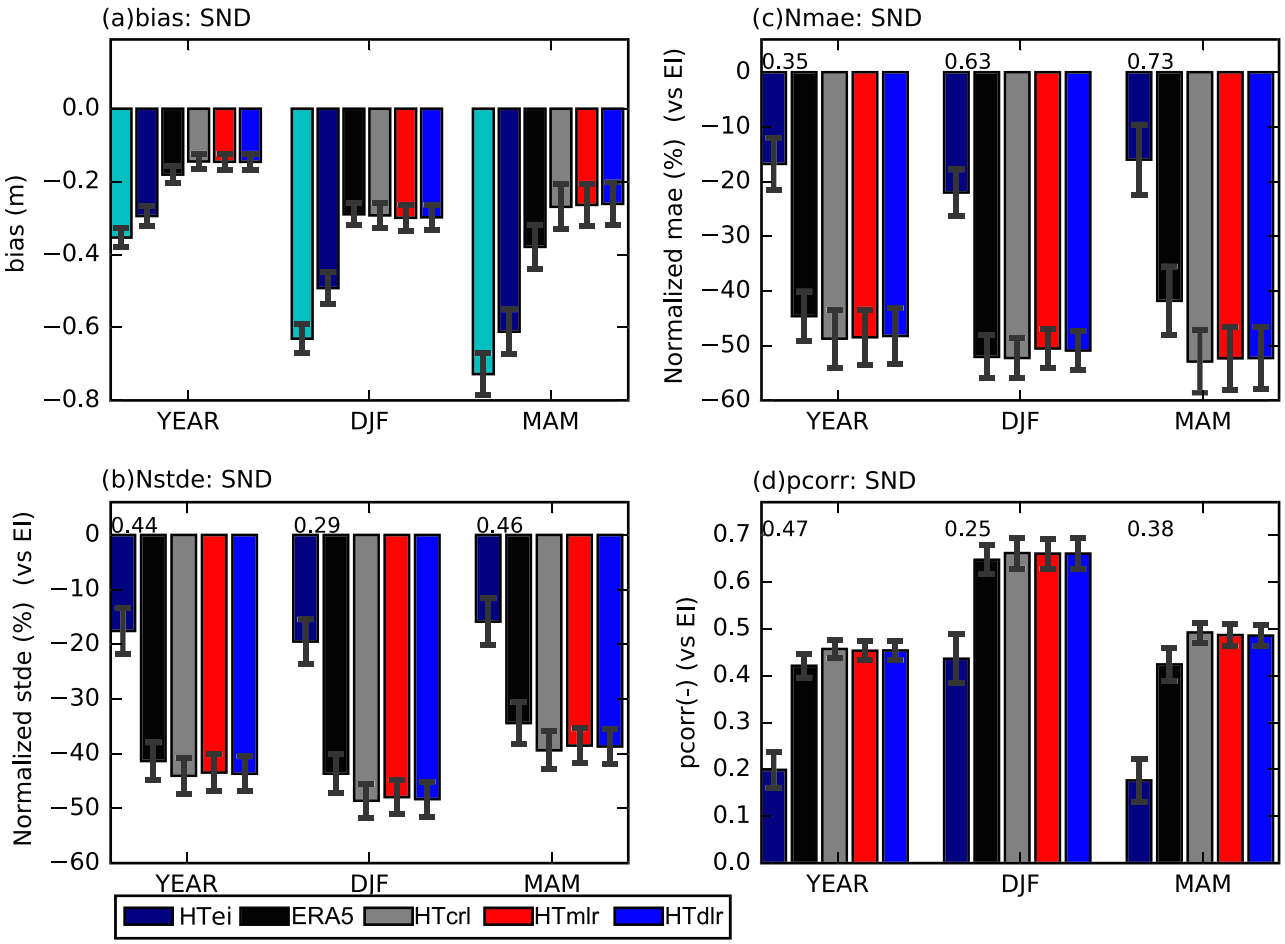

Figure 7. As Figure 6 but for snow depth. The horizontal axis shows the scores for the full period (YEAR), only winter (DJF), and only spring (MAM). The statistics were computed using 313 stations with a mean elevation difference between ERA5 orography and the stations of −413 m.

in ERA5, and 52% in HTclr/HTmlr/HTdlr. As for the soil temperatures, there is no clear difference between the different methods of ELR temperature corrections.

3.4. Station Representativity

Comparing model simulations with in situ observations raises several questions regarding spatial representativity. Models normally represent a certain quantity as the mean over a grid box while in situ observations are local and, depending on the weather conditions and location, their spatial representativity can vary significantly. This raises questions as follows: What is the representativity uncertainty of the in situ data, and how does this varies with the spatial scale considered? Considering the reasonably high-density network over the considered WUS region, an estimate of the spatial uncertainty derived from observations was carried out as described in section 2. The results applied to the GHCN dtmin, dtmean, and dtmax (see Figure 8) provide an estimate of the in situ representativity uncertainty. This can be also interpreted as the minimum MAE and STDE that should be expected when comparing grid-averaged versus individual stations. This could be further interpreted as the minimum expected errors (or benchmark) when comparing model data with the in situ observations; that is, we should not expect a MAE or STDE of 0 but a minimum value associated with the station sampling and characteristics. The results (in Figure 8) show that both MAE and STDE increase with increased radius (i.e., larger areas) and are larger for dtmax than for dtmin and dtmean has the lower values. The dtmax and dtmin MAE becomes similar when considering only stations with similar altitudes (comparing Figure 8b solid vs. dashed red and blue lines). This indicates a higher sensitivity the daily maximum temperature to elevation difference than daily minimum temperature. The large STDE of dtmax, when compared with dtmin, is partially associated with a larger temporal variability (day to day) of dtmax.

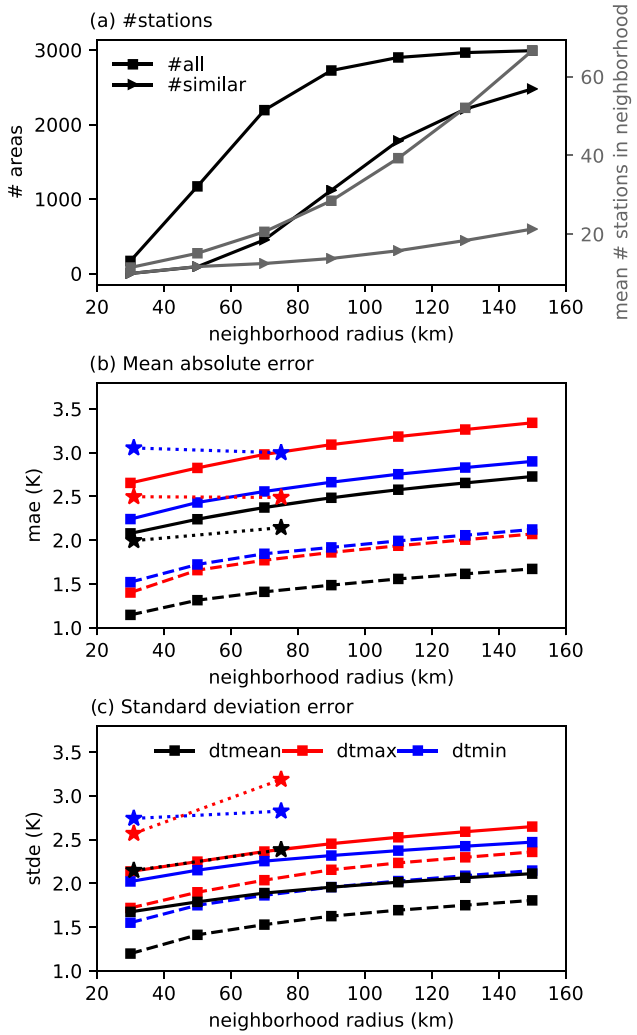

Figure 8. Observation temperature errors estimate dependence on resolution. (a) The number of areas used for each search radius (left axis, black) and mean number of stations in each (right axis, gray), considering all stations (squares) in a neighborhood radius (horizontal axis) or only stations in the neighborhood with a similar altitude (within 100 m, in triangles). Estimate of mean absolute error (b) and standard deviation of the error (c) of the mean compared with the neighborhood stations for different search radius. In panels (b) and (c) the colors indicate dtmean (black), dtmax (red), and dtmin (blue) while the solid lines indicate that all stations in the neighborhood radius are used while dashed lines indicate that only stations with a similar altitude were considered. Panels (b) and (c) also show the error estimates of ERAI (at 75 km) and ERA5 (at 31 km) as stars connected by a dotted line. The ERAI and ERA5 estimates were computed only for stations with an altitude difference lower than 100 m to both ERAI and ERA5 orography (588 stations).

The altitude differences explain almost 50% of the MAE while for the STDE, the impact of altitude differences is smaller. These results are expected as systematic differences driven by altitude are significant while random differences are associated with local effects where altitude alone does not explain the differences.

By comparing ERAI and ERA5 errors with the observational MAE and STDE estimates, it is possible to assess on one hand the evolution of the reanalysis and on the other hand how far the reanalysis is from the expected minimum. For this comparison, only stations with altitude differences lower than 100 m to both ERAI and ERA5 orography were considered (588 stations). Since the reanalysis metrics are computed only for stations with similar altitudes, the benchmark values (or lower limits) should be the estimates using only stations with similar altitudes (dashed lines in Figures 8b and 8c). For the MAE, there was a slight increase of the error from ERAI to ERA5 of dtmin and dtmax with a slight reduction of dtmean. In the case

of the STDE there was a clear reduction from ERAI to ERA5, particularly for dtmax. The reduction of the STDE highlights the model and data assimilation advances in reducing random errors from ERAI to ERA5, likely associated with synoptic variability. However, the stagnation of the systematic errors despite model and resolution enhancements suggests that further focus on model processes (e.g., land surface, boundary layer, clouds, and radiation) is still required.

4. Conclusions

The use of the in situ GHCN network to estimate the ELR shows a clear annual cycle as well as diurnal variations, with lower ELR for dtmin when compared with dtmax and higher values during summer (JJA) when compared with winter (DJF). These results are consistent with the findings of Minder et al. (2010) over the Cascade Mountains. The estimated ELR from ERA5 vertical profiles is reasonably consistent with the observational data, both temporally and spatially, when using dtmean, with a tendency for overestimation. The proposed methodology to derive the ELR from ERA5 vertical profiles only provides a daily mean estimate, which is a limitation considering the striking variability seen in the observations between daily maximum and minimum temperatures and ELR. Inversions are neglected, contributing to the overestimation of the derived ELR and limiting its application in typical inversion conditions (e.g., clear-sky cold nights).

The elevation correction of ERA5 temperature to the GHCN stations elevation using different ELR corrections (from constant to daily varying fields) showed that there is no single approach outperforming the others consistently. However, considering the daily mean temperature, the temporally and spatially varying ELR derived from ERA5 vertical profiles (mlr and dlr) provides the best correction by removing most of the error dependence on altitude. However, when evaluating the temperature elevation corrections to station altitude, there is no significant added value of the variable ELR when compared with the constant ELR. Additionally, the performance of the corrections for dtmin and dtmax and for stations below or above the model orography varies significantly. Our results highlight the drawbacks of the simple ELR correction (even when considering a spatially and temporally varying ELR), which fails to capture changes in the diurnal temperature range, as well as local effects. In all cases, the temporally and spatially varying ELR (mlr and dlr) leads to an increase of the random error (standard deviation of the error), which is a considerable limitation of this approach. Therefore, the use of this approach when correcting model data to a particular location is mainly suitable for the daily mean temperature, while caution must be taken for daily minimum and maximum temperatures. The systematic biases in ERA5 are due to both local effects, which are not strictly dependent on altitude (Pepin, 2005; Steinacker et al., 2007; Vosper & Brown, 2008), and physical processes representation in the model (e.g., radiation, boundary layer, and surface heterogeneities), leaving altitude differences as a second-order effect to explain the mixed impact of the ELR corrections tested.

The response of the land surface to the altitude changes was evaluated by downscaling ERA5 near-surface meteorology to drive the land surface model, accounting for different ELR corrections in temperature. The validation was focused on the SNOTEL network of snow depth and 5-cm deep soil temperature, comparing the evolution from ERAI to ERA5 and the surface high-resolution (9 km) simulations. For soil temperatures, there is a clear improvement from ERAI to ERA5 with the surface downscaling further improving the standard deviation of the error and temporal correlations during winter. For snow depth, the added value of the surface simulations when compared with ERA5 is mainly restricted to the melting season. This surface-only downscalling methodology can also benefit from other corrections. An example would be precipitation, considering the recent advances in generating multiproduct precipitation estimates (Beck et al., 2019). Other corrections such as downward solar radiation shading by topography (Varley et al., 1996) or rainfall/snowfall partitioning (Tobin et al., 2012) could be also explored.

By comparing the estimated representativity errors of the in situ GHCN temperature observations with the ERAI, ERA5, and downscaled errors, the improvements from ERAI to ERA5 were reasonably limited (considering the expected improvements by resolution alone) and mainly in the random component of the error. Despite the significant efforts in modeling and data assimilation, the representation of near-surface temperature in the reanalysis is challenging, in particular for daily minimum temperatures. This is likely associated with a large range of limitations in the model representation of clouds, radiation, boundary layer, and land surface characteristics, among others. While the random component of the errors was improved in ERA5, likely due to a better synoptic scale variability and resolution, the still significant systematic biases require further attention from the modeling perspective.

Acknowledgments
The ERAI reanalysis is available from ECMWF data archive: https://apps.ecmwf.int/datasets/data/interim-full-daily/. ERA5 dataset is available from the Copernicus Climate Change Service: https://climate.copernicus.eu/climate-reanalysis. The observational GHCN dataset was accessed from: https://www.ncdc.noaa.gov/ghcnd-data-access, and the SNOTEL from: https://www.wcc.nrcs.usda.gov/snow/. The surface simulations carried out in this study are available from ECMWF data archive (required login at: https://apps.ecmwf.int/mars-catalogue/?class=rd) with the research experimental Ids: got2(HTbil), gote(HTdlr), gotf(HTclr), gpob(HTmlr), gpb1 (HTei). This study was funded by the FCT project CONTROL PTDC/CTA-MET/28946/2017. E. Dutra acknowledges the financial support of FCT research grant IF/00817/2015. The authors acknowledge two anonymous reviewers for their constructive comments and suggestions.

References

Albergel, C., Dutra, E., Munier, S., Calvet, J.-C., Munoz-Sabater, J., Rosnay, P. d., & Balsamo, G. (2018). ERA-5 and ERA-Interim driven ISBA land surface model simulations: Which one performs better? *Hydrology and Earth System Sciences*, *22*(6), 3515–3532. https://doi.org/10.5194/hess-22-3515-2018

Albergel, C., Dutra, E., Muñoz-Sabater, J, Haiden, T., Balsamo, G., Beljaars, A., et al. (2015). Soil temperature at ECMWF: An assessment using ground-based observations. *Journal of Geophysical Research: Atmospheres*, *120*, 1361–1373. https://doi.org/10.1002/2014jd022505

Balsamo, G., Albergel, C., Beljaars, A., Boussetta, S., Brun, E., Cloke, H., et al. (2015). ERA-Interim/Land: A global land surface reanalysis data set. *Hydrology and Earth System Sciences*, *19*, 389–407. https://doi.org/10.5194/hess-19-389-2015

Balsamo, G., Viterbo, P., Beljaars, A., Van den Hurk, B., Betts, AK, & Scipal, K. (2009). A revised hydrology for the ECMWF model: Verification from field site to terrestrial water storage and impact in the integrated forecast system. *Journal of Hydrometeorology*, *10*, 623–643. https://doi.org/10.1175/2008JHM1068.1

Bechtold, P., Köhler, M., Jung, T., Doblas-Reyes, F., Leutbecher, M., Rodwell, M. J., et al. (2008). Advances in simulating atmospheric variability with the ECMWF model: From synoptic to decadal time-scales. *Quarterly Journal of the Royal Meteorological Society*, *134*(634), 1337–1351. https://doi.org/10.1002/qj.289

Beck, H. E., Pan, M., Roy, T., Weedon, G. P., Pappenberger, F., van Dijk, A. I. J. M., et al. (2019). Daily evaluation of 26 precipitation datasets using stage-IV gauge-radar data for the CONUS. *Hydrology and Earth System Sciences*, *23*(1), 207–224. https://doi.org/10.5194/hess-23-207-2019

Behnke, R., Vavrus, S., Allstadt, A., Albright, T., Thogmartin, W. E., & Radeloff, V. C. (2016). Evaluation of downscaled, gridded climate data for the conterminous United States. *Ecological Applications*, *26*(5), 1338–1351. https://doi.org/10.1002/15-1061

Bernier, N. B., Belair, S., Bilodeau, B., & Tong, L. (2011). Near-surface and land surface forecast system of the Vancouver 2010 winter olympic and paralympic games. *Journal of Hydrometeorology*, *12*, 508–530. https://doi.org/10.1175/2011jhm1250.1

Cao, B., Gruber, S., & Zhang, T. (2017). REDCAPP (v1.0): Parameterizing valley inversions in air temperature data downscaled from reanalyses. *Geoscientific Model Development*, *10*(8), 2905–2923. https://doi.org/10.5194/gmd-10-2905-2017

Cosgrove, B. A., Lohmann, D., Mitchell, K. E., Houser, P. R., Wood, E. F., Schaake, J. C., et al. (2003). Real-time and retrospective forcing in the North American Land Data Assimilation System (NLDAS) project. *Journal of Geophysical Research*, *108*(D22), 3. https://doi.org/10.1029/2002JD003118

Dall'Amico, M., & Hornsteiner, M. (2006). A simple method for estimating daily and monthly mean temperatures from daily minima and maxima. *International Journal of Climatology*, *26*(13), 1929–1936. https://doi.org/10.1002/joc.1363

Dee, D. P., Uppala, S. M., Simmons, A. J., Berrisford, P., Poli, P., Kobayashi, S., et al. (2011). The ERA-Interim reanalysis: Configuration and performance of the data assimilation system. *Quarterly Journal of the Royal Meteorological Society*, *137*(656), 553–597. https://doi.org/10.1002/qj.828

Dodson, R., & Marks, D. (1997). Daily air temperature interpolated at high spatial resolution over a large mountainous region. *Climate Research*, *8*, 1–20. https://doi.org/10.3354/cr008001

Dutra, E., Balsamo, G., Viterbo, P., Miranda, PMA, Beljaars, A., Schar, C., & Elder, K. (2010). An improved snow scheme for the ECMWF land surface model: Description and offline validation. *Journal of Hydrometeorology*, *11*, 899–916. https://doi.org/10.1175/2010JHM1249.1

Dutra, E., Schär, C., Viterbo, P., & Miranda, P. M. A. (2011). Land-atmosphere coupling associated with snow cover. *Geophysical Research Letters*, *38*, L15707. https://doi.org/10.1029/2011gl048435

Endris, H. S., Omondi, P., Jain, S., Lennard, C., Hewitson, B., Chang'a, L., et al. (2013). Assessment of the performance of CORDEX regional climate models in simulating East African rainfall. *Journal of Climate*, *26*(21), 8453–8475. https://doi.org/10.1175/JCLI-D-12-00708.1

Gao, L., Bernhardt, M., & Schulz, K. (2012). Elevation correction of ERA-Interim temperature data in complex terrain. *Hydrology and Earth System Sciences*, *16*, 4661–4673. https://doi.org/10.5194/hess-16-4661-2012

Gao, L., Bernhardt, M., Schulz, K., & Chen, X. (2017). Elevation correction of ERA-Interim temperature data in the Tibetan Plateau. *International Journal of Climatology*, *37*(9), 3540–3552. https://doi.org/10.1002/joc.4935

Gerlitz, L., Conrad, O., Thomas, A., & Böhner, J. (2014). Warming patterns over the Tibetan Plateau and adjacent lowlands derived from elevation- and bias-corrected ERA-Interim data. *Climate Research*, *58*(3), 235–246.

Hersbach, H., de Rosnay, P., Bell, B., Schepers, D., Simmons, A., Soci, C., et al. (2018). Operational global reanalysis: Progress, future directions and synergies with NWP. *ECMWF ERA Report Series*, *27*, 65. https://www.ecmwf.int/node/18765, .

Ioannidou, L., Yu, W., & Bélair, S (2014). Forecasting of surface winds over eastern Canada using the Canadian offline land surface modeling system. *Journal of Applied Meteorology and Climatology*, *53*(7), 1760–1774. https://doi.org/10.1175/JAMC-D-12-0284.1

Jobst, A. M., Kingston, D. G., Cullen, N. J., & Sirguey, P. (2017). Combining thin-plate spline interpolation with a lapse rate model to produce daily air temperature estimates in a data-sparse alpine catchment. *International Journal of Climatology*, *37*(1), 214–229. https://doi.org/10.1002/joc.4699

Liston, G. E., & Elder, K. (2006). A meteorological distribution system for high-resolution terrestrial modeling (MicroMet). *Journal of Hydrometeorology*, *7*(2), 217–234. https://doi.org/10.1175/JHM486.1

Maraun, D., Wetterhall, F., Ireson, A. M., Chandler, R. E., Kendon, E. J., Widmann, M., et al. (2010). Precipitation downscaling under climate change: Recent developments to bridge the gap between dynamical models and the end user. *Reviews of Geophysics*, *48*, RG3003. https://doi.org/10.1029/2009RG000314

Maselli, F., Pasqui, M., Chirici, G., Chiesi, M., Fibbi, L., Salvati, R., & Corona, P. (2012). Modeling primary production using a 1 km daily meteorological data set. *Climate Research*, *54*(3), 271–285.

Maurer, E. P., Wood, A. W., Adam, J. C., Lettenmaier, D. P., & Nijssen, B. (2002). A long-term hydrologically based dataset of land surface fluxes and states for the conterminous United States. *Journal of Climate*, *15*(22), 3237–3251. https://doi.org/10.1175/1520-0442(2002)015<3237:ALTHBD>2.0.CO;2

Menne, M. J., Durre, I., Korzeniewski, B., McNeal, S., Thomas, K., Yin, X., et al. (2012). Global Historical Climatology Network—Daily (GHCN—Daily), Version 3. Title of the publication associated with this dataset: https://data.nodc.noaa.gov/cgi-bin/iso?id=gov.noaa.ncdc:C00861, .

Menne, M. J., Durre, I., Vose, R. S., Gleason, B. E., & Houston, T. G. (2012). An overview of the Global Historical Climatology Network—Daily database. *Journal of Atmospheric and Oceanic Technology*, *29*(7), 897–910. https://doi.org/10.1175/JTECH-D-11-00103.1

Minder, J. R., Mote, P. W., & Lundquist, J. D. (2010). Surface temperature lapse rates over complex terrain: Lessons from the cascade mountains. *Journal of Geophysical Research*, *115*, F02011. https://doi.org/10.1029/2009JD013493

Pepin, N. C. (2005). A global comparison of surface and free-air temperatures at high elevations. *Journal of Geophysical Research*, *110*, D03104. https://doi.org/10.1029/2004JD005047

Shen, Y.-J., Shen, Y., Goetz, J., & Brenning, A. (2016). Spatial-temporal variation of near-surface temperature lapse rates over the Tianshan mountains, central Asia. *Journal of Geophysical Research: Atmospheres*, *121*, 14,006–14,017. https://doi.org/10.1002/2016JD025711

Sheridan, P., Smith, S., Brown, A., & Vosper, S. (2010). A simple height-based correction for temperature downscaling in complex terrain. *Meteorological Applications*, *17*, 329–339. https://doi.org/10.1002/met.177

Soares, P. M. M., Cardoso, R. M., Lima, D. C. A., & Miranda, P. M. A. (2017). Future precipitation in portugal: High-resolution projections using WRF model and EURO-CORDEX multi-model ensembles. *Climate Dynamics*, *49*(7-8), 2503–2530. https://doi.org/10.1007/s00382-016-3455-2

Soares, P. M. M., Cardoso, R. M., Miranda, P. M. A., de Medeiros, J., Belo-Pereira, M., & Espirito-Santo, F. (2012). WRF high resolution dynamical downscaling of ERA-Interim for Portugal. *Climate Dynamics*, *39*(9), 2497–2522. https://doi.org/10.1007/s00382-012-1315-2

Stahl, K., Moore, R. D., Floyer, J. A., Asplin, M. G., & McKendry, I. G. (2006). Comparison of approaches for spatial interpolation of daily air temperature in a large region with complex topography and highly variable station density. *Agricultural and Forest Meteorology*, *139*(3), 224–236. https://doi.org/10.1016/j.agrformet.2006.07.004

Steinacker, R., Whiteman, . CD., Dorninger, M., Pospichal, B., Eisenbach, S., Holzer, A. M., et al. (2007). A sinkhole field experiment in the eastern alps. *Bulletin of the American Meteorological Society*, *88*(5), 701–716. https://doi.org/10.1175/BAMS-88-5-701

Tobin, C., Rinaldo, A., & Schaefli, B. (2012). Snowfall limit forecasts and hydrological modeling. *Journal of Hydrometeorology*, *13*(5), 1507–1519. https://doi.org/10.1175/JHM-D-11-0147.1

Varley, M. J., Beven, K. J., & Oliver, H. R. (1996). Modelling solar radiation in steeply sloping terrain. *International Journal of Climatology*, *16*(1), 93–104. https://doi.org/10.1002/(SICI)1097-0088(199601)16:1<93::AID-JOC992>3.0.CO;2-T

Vosper, S. B., & Brown, A. R. (2008). Numerical simulations of sheltering in valleys: The formation of nighttime cold-air pools. *Boundary-Layer Meteorology*, *127*(3), 429–448. https://doi.org/10.1007/s10546-008-9272-3

Wang, Y., Wang, L., Li, X., & Chen, D. (2018). Temporal and spatial changes in estimated near-surface air temperature lapse rates on tibetan plateau. *International Journal of Climatology*, *38*, 2907–2921. https://doi.org/10.1002/joc.5471

Weiss, A., & Hays, C. J. (2005). Calculating daily mean air temperatures by different methods: Implications from a non-linear algorithm. *Agricultural and Forest Meteorology*, *128*(1), 57–65. https://doi.org/10.1016/j.agrformet.2004.08.008

Winstral, A., Jonas, T., & Helbig, N. (2017). Statistical downscaling of gridded wind speed data using local topography. *Journal of Hydrometeorology*, *18*(2), 335–348. https://doi.org/10.1175/JHM-D-16-0054.1